Extended Abstracts of the 2006 International Conference on Solid State Devices and Materials, Yokohama, 2006, pp. 628-629

P-6-9

A Size-Dependent Equivalent-Circuit Model of High Performance Near-Ballistic-Transport Photodiode

Y.-S. Wu[1], D.-M. Lin[1], F.-H. Huang[1], W. Y. Chiu[1], J.-W. Shi[1*], Y.-J. Chan[1]

[1]Department of Electrical Engineering, National Central University
Taoyuan 320, TAIWAN, R.O.C.
Tel: +886-3-4227151 ext. 34466 FAX:+886-3-4255830 Email: jwshi@ee.ncu.edu.tw

1. Introduction

In this paper, we developed an analytical equivalent-circuit-model, which includes the RC-delay time and carrier transport time, to investigate the distinct dynamic behaviors of the Near-Ballistic Uni-Traveling-Carrier Photodiode (NBUTC-PD) with different geometry sizes [1]. This device, in which the structure of the collector of the Uni-Traveling-Carrier PD is modified, can achieve excellent performance at a 1.55μm wavelength. According to the measured frequency responses of the scattering (S) parameters of NBUTC-PD and detailed device-modeling, the observed enhancement of the net optical-to-electrical (O-E) bandwidth under high-power operation will depend on the active areas of device seriously and can be attributed to the unique near-ballistic-transport property of the photo-generated electron, which has never been observed in the traditional high-speed, high-power photodiode. The obvious size-dependent bandwidth enhancement phenomenon of NBUTC-PD indicates its applicability in nonlinear optoelectronic mixer and analog fiber communication system with high linearity requirement by use of the devices with large (~300μm^2) and small (~100μm^2) active areas, respectively.

3. Equivalent Circuit

The bandwidth of a PD is determined by the carrier transport time ($1/f_t$), and the RC time constant ($1/f_{RC}$), and the net O-E bandwidth (f_{3dB}) can be approximated as (1): $\frac{1}{f_{3dB}^2}=\frac{1}{f_{RC}^2}+\frac{1}{f_t^2}$ (1)
In order to study the observed significant bandwidth enhancement phenomenon based on the dominate points of RC limitation and the internal carrier dynamics, we adopted an equivalent-circuit-model [2], which included these three effects, as shown in Figure 1. The detail of this model is given in our previous work [2]. Region 1 and region 2 represent the bandwidth limitation of the carrier transit time (f_t) and the space charge screen effect, and RC delay time (f_{RC}), respectively. In region 2, C_{suff} is the capacitance of the E layer, R_p is the sum of the p-electrode contact resistance and the resistance of the P layer, R_n is the contact resistance of the n-electrode, L and C_p are the CPW pad inductance and capacitance, respectively, and C_{dx} is the parasitic capacitance between the p-electrode and n-electrodes. The shunted C_{co} and R_{co} represent the displacement current and conduction current in the collector layer, respectively. The frequency dependent ac photocurrent I(f), which is the current source of region 2, can be represented by the voltage (V_{RF})-controlled-current-source (g_mV_{RF}). The frequency response of V_{RF} (V_{RF}(f)) is determined by the product of R_tC_t, and the fixed constant g_m represents the optical-to-RF conversion quantum efficiency. In region 1, we use an artificial RC network (R_t and C_t) to mimic the bandwidth limitation of the carrier transit time. In our modeling process, we can determine the RC equivalent-circuit-model (region 2) first by using the measured (S_{22}) parameters and then use the measured O-E frequency response (S_{21}) with the extracted RC network (region 2) to determine the values of R_t, C_t. By using the extracted R_t and C_t, we can further determine the effective drift-velocity of the carrier according the reported formula (2): $\frac{1}{2\pi R_tC_t}=0.55\frac{v_e}{d}$ (2), where d is the total drift distance of the carrier and v_e is the average drift-velocity of an electron. For our devices, we assume that d is equal to 450nm, which includes the thicknesses of the P layer (150nm), C layer (200nm), and E layer (100nm).

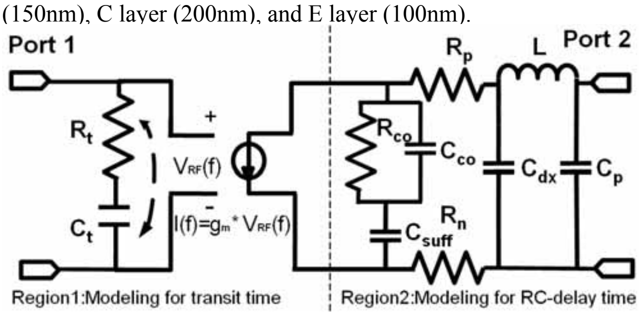

Fig. 1 Small-signal ration frequency model of NBUTC-PD that involves the parasitic elements, carrier transit-time effect.

3. Measurement Results

The measured f_{3dB} electrical bandwidths of BUTC-PD with a 320μm^2 and a 160μm^2 active area under different reverse bias voltages and output photocurrents were shown in Fig. 2(a) and (b), respectively. The maximum measured photocurrent in these two figures was limited by the device failure. As shown in these two figures, we can see that as the reverse bias voltage increased (-2V, -3V, and -5V), both devices revealed different dynamic behaviors.

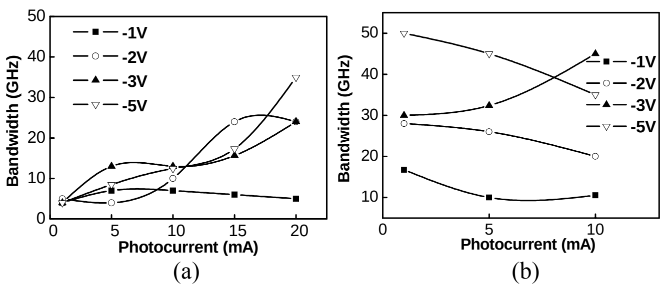

Fig. 2 Electrical bandwidth versus photocurrent under different bias voltages of the device with a 320μm^2 active area (close square: -1V; open circle: -2V; close triangle: -3V; open triangle: -5V) (a) with a 320μm^2 active area, and (b) with a 160μm^2 active area.

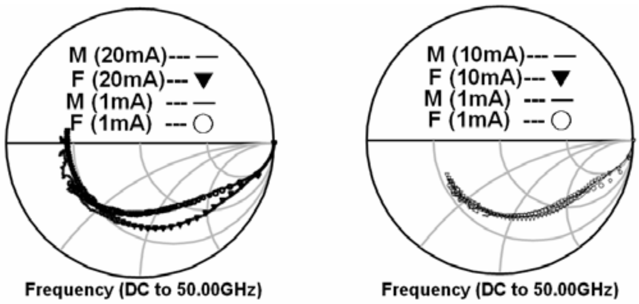

(a) (b)

Fig. 3 The measured and the fitted S_{22} parameters of the device with a 320μm^2 active area (a) and a 160μm^2 active area (b) under different levels of output photocurrent and a fixed bias voltage -3V.

Figure 3 (a) and (b) shows the fitted and measured S_{22} parameters of devices with 320μm^2 and 160μm^2 active areas, respectively under different output photocurrents (1mA and 20mA for large device; 1mA and 10mA for small device) and fixed bias voltage -3V. In comparison of Fig. 3(a) and Fig. 3(b), the difference between the S_{22} parameters of large device under low and high photocurrents is much obvious then that of small device is. The variation of S_{22} parameters can be attributed to the change of the elements' values in the region 2 of equivalent-circuit-model.

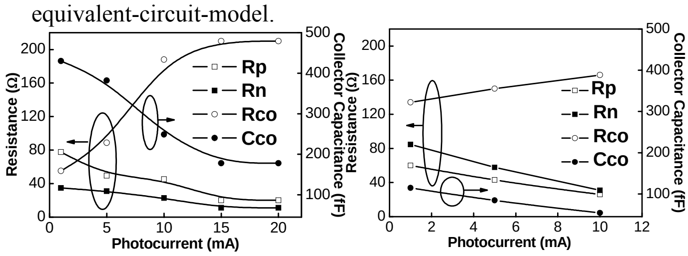

(a) (b)

Fig. 4 The extracted values of the circuit elements under a fixed bias voltage -3V and different levels of output photocurrent for large device (a), and small device (b).

As shown in Fig. 4, both cases show the same trend of increase in R_{co} and of reduction in C_{co} as photocurrent increase besides the varying range is different from each other. Regarding the reduction of C_{co}, it is due to the subtraction of the differential AC capacitance $I_c\times(d\tau_c/dV)$, proportional to the current, from the depletion capacitance [2,3], where, V_{ac} is the output ac voltage, I_C is the photocurrent, and τ_c is the electron drift time. As far as the same scale of photocurrent density that changed from 1mA to 10mA for small size device and from 1mA to 20mA for large size is concerned, the collector junction capacitance of large device decrease from 430fF to 178fF, but of small device just decrease from 114fF to 54fF which changes much smaller then large device. By utilizing the obtained RC network and the measured O-E frequency responses (S_{21}), we can further determine the values of the circuit elements in region 1 and extract the carrier transit time. The fitted average electron transit time, which is equal to $2\pi R_tC_t$, and the extracted average electron drift-velocity of large device and of small device under different output photocurrent densities are shown in Figure 5(a) and (b), respectively. We can clearly see that the drift-velocity increases from about 2.2×10^{7}cm/s to 4×10^{7}cm/s as the photocurrent density increases from 625A/cm^2 to 6250A/cm^2 has been observed in large device. Compared with large device, the drift-velocity of small device increases from 2.8×10^{7}cm/s to 4×10^{7}cm/s under the same scale of photocurrent density is similar to large device. Up to now, it is enough to prove that the vibration of the AC capacitance, which dominates the size dependent bandwidth enhancement phenomenon of NBUTC-PD, is strongly influenced by the change of output photocurrent. The maximum output photocurrent of large device usually lager then that of small device, so that it's nonlinear properties is also much stronger then small one under the same photocurrent density.

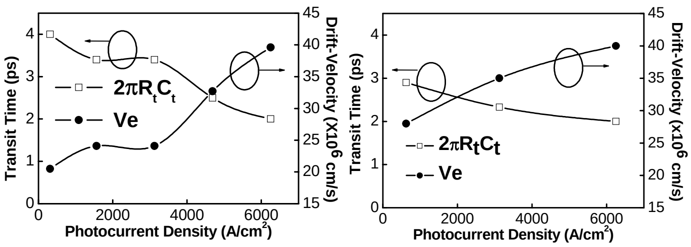

(a) (b)

Fig. 5 The extracted values of the transit time and average drift-velocity under different levels of output photocurrent for large device (a), and small device (b).

4. Conclusions

In conclusion, we have analyzed the dynamic behaviors of NBUTC-PD with different size of active region. With use of the extracted S parameters and equivalent-circuit-model fitting, the size dependent bandwidth enhancement can be attributed to different initial total capacitance, and different degree of AC reduction capacitance associate with the maximum output photocurrent. According to our results, the NBUTC-PD can be extensively applied in not only optoelectronic mixer [4], but also analog fiber communication due to the appearance of bandwidth enhancement phenomenon can be modified by adjusting the device size. The observed high permanence, and adjustable near-ballistic operation may play an important role in the development of next-generation ultra-high speed PD.

Acknowledgments

The authors are grateful to the financial support from the MOE Program for Promoting Academic Excellence of Universities. (Grant number 91-E-FA06-1-4), and the Ministry of Economic Affairs of Republic of China under the Program for Industrial Technology Development (NSC-95-2215-E-008-003).

References

[1] J.-W. Shi and Y.-S. Wu, *IEEE Photon. Technol. Lett.*, **17** (2005) 1929.

[2] Y.-S. Wu and J.-W. Shi, *IEEE Photon. Technol. Lett.*, **18** (2006) 938.

[3] M. Achouche and V. Magnin, *IEEE Photon. Technol. Lett.*, **16**(2004)584.

[4] M. Tsuchiya, and T. Hosida, *IEEE Trans. Microwave Theory Tech.,* **49** (1999) 1432.